Role of oxygen defects in inducing the blue photoluminescence of zinc oxide films deposited by magnetron sputtering

Kun Chen (陈 坤)[1], Huanfeng Zhu (朱焕锋)[1], Xinyu Yi (易歆雨)[1], Shuai Cheng (程 帅)[1], Jing Li (李 晶)[1,2,*], Songyou Wang (王松有)[1,2], Ming Lu (陆 明)[1,2], Min Xu (徐 敏)[1,2], Li Ma (马 丽)[3], and Lei Lü (吕 磊)[4]

[1]*Department of Optical Science and Engineering, Fudan University, Shanghai Ultra-Precision Optical Manufacturing Engineering Center, Shanghai 200433, China*

[2]*Key Laboratory of Micro and Nano Photonic Structures (Ministry of Education), Shanghai 200433, China*

[3]*College of Physical Science and Engineering, Tongji University, Shanghai 200092, China*

[4]*Department of Medical Physics, Weifang Medical University, Shandong 261053, China*

**Corresponding author: lijing@fudan.edu.cn*

Received April 18, 2015; accepted August 19, 2015; posted online September 9, 2015

A number of zinc oxide (ZnO) films are deposited on silicon substrates using the magnetron sputtering method. After undergoing thermal treatment under different conditions, those films exhibit hexagonal wurtzite structures and different photoluminescent characteristics. Besides the notable ultraviolet emission, which is related to the free exciton effect, a distinct blue fluorescence around 475 nm is found in some special samples. The blue photoluminescence emission of the ZnO film is believed to be caused by oxygen vacancies.

OCIS codes: 310.6860, 310.1860, 300.6280, 260.3800.
doi: 10.3788/COL201513.103101.

Zinc oxide (ZnO) is an important II–VI group compound semiconductor that has attracted a lot of interest. Due to its wide, direct bandgap of 3.3 eV at 300 K, ZnO plays an outstanding role in the field of optoelectronic applications[1–3]. Not only does it have applications in short-wavelength, light emitting and detecting devices, but also it has adequate potential in applications involving the visible region of light[4,5]. Furthermore, ZnO is an ideal component of nanoscale devices due to its functional morphologies[6–8]. Photoluminescence (PL) is an efficient method that is usually used to analyze the characteristics of materials. The PL spectrum of ZnO consists of a well-known, near-band-edge (NBE) emission and a deep level (DL) emission, which involves the blue, green, yellow, orange, and red bands[4–6,9–21]. The strong NBE emission is extremely important for ultraviolet (UV) optoelectronic applications, such as light emitting diodes and laser diodes. Defects sufficiently influence the electrical and optical properties of ZnO.

However, the origin and mechanism of the DL emission is still controversial. Many researchers have tried to explain the origin of the DL emission. Moore *et al.* indicated that the blue emission of ZnO films prepared by thermal oxidation was related to zinc interstitials (Zn_i) found within the depletion region near the surface[14]. Green luminescence has been widely observed. Heo *et al.* assigned the green emission to donor-deep acceptor (zinc vacancy, V_{Zn}^{-}) transitions, and the yellow emission to donor-deep acceptor (oxygen interstitial, O_i^{-}) transitions[15]. Studenikin *et al.* proposed that the green PL spectrum of ZnO was the electron hole recombination involving a donor-acceptor complex, which consists of an oxygen vacancy (V_o) and a zinc vacancy (V_{Zn})[17]. Lin *et al.* reported that the green emission is correlated with the electron transition from the bottom of the conduction band to the oxygen antisite defect (O_{Zn}) level[20]. Also, it was proposed that extrinsic impurities generate green luminescence[22]. The orange emission was detected in oxygen-rich ZnO films obtained by annealing in oxygen[16]. The yellow emission can be attributed to the conduction band with a deep electron close to the conduction band and a deeply trapped hole in the O_i^{-} center[20]. The Li-doped ZnO films exhibited yellow luminescence with a peak at about 2.2 eV[18]. A red luminescence band appeared in the PL spectrum of undoped bulk ZnO after a post-annealing at 700°C in air[13]. In this Letter, the multiple emission bands of ZnO films involving UV and DL emission were investigated. Also, the origin of the blue emission was discussed carefully. An unusual understanding of the blue emission was obtained in this research.

The ZnO films were deposited onto silicon substrates using a ZnO target with a purity of 99.999% by the direct current magnetron sputtering system. The sputtering power was set at 100 W. The background vacuum was 6.5×10^6 mbar, and the working vacuum was about 3.3×10^3 mbar. With a deposition rate of 0.24 nm/s and a growth time of 1500 s, the thickness of the as-deposited films was about 360 nm. Thermal treatments were applied to the as-deposited films both in nitrogen (99.999%) and in air at different temperatures and processing times in a tubular furnace. The annealing temperatures were 500°C, 700°C, and 900°C. The samples were kept in nitrogen or

air after annealing until the furnace cooled down to room temperature. The names of those annealed ZnO samples follow the abbreviation "N/A TTTtt" in this Letter. "N" represents the sample annealed in nitrogen, "A" is the sample annealed in air, "TTT" is the annealing temperature, and "tt" is the annealing time. For example, "N50060" represents the sample annealed at 500°C for 60 min in nitrogen, and "A90005" stands for the sample annealed at 900°C for 5 min in air.

X ray diffraction (XRD) was employed to characterize the crystalline structures of all prepared ZnO films. The XRD patterns show that the annealed films had a typical hexagonal wurtzite structure[4,7,11,13,23], as shown in Fig. 1(a). Here, the annealing ambience (in N_2 or in air) does not change the crystalline properties of the films much. Instead, the annealing temperature and time have a great influence on the XRD results. For the films annealed at 500°C and 700°C, two peaks (002) and (103) are observed around the angles of 34.4° and 63.0°. When the annealing temperature increases, the peak (002) is suppressed, and the peak (103) is enhanced. This is because ZnO nanoparticles are more likely to grow along the (103) orientated axis. When the films are annealed at 900°C, the same variation tendency is observed for the two resulting peaks. Additionally, another two weak peaks (102) and (110) appear at 47.8° and 54.6°. When the annealing time was changed for our samples, the grain sizes increased slightly [see Fig. 1(b)]. The films annealed in air are larger in size than those annealed in nitrogen (seen from the samples annealed at 500°C and 900°C) because the existence of defects is unfavorable for the grains to grow. The grain size deduced from the (103) peak using the Debye-Scherrer formula is illustrated in Fig. 1(b). The annealing time for each sample has been labeled beside the data points in Fig. 1(b). The Debye-Scherrer formula can be expressed as

$$D_{hkl} = \beta\lambda / B \cos\theta, \tag{1}$$

where D_{hkl} is the grain diameter along the axis (hkl); β is a constant and equals 0.89 for those grain sizes that are less than 100 nm in accordance with practice; λ is the working wavelength of 0.15418 nm in the XRD system; B is the full width of the half height of the peak chosen to perform the calculation, and 2θ is the angle detected as corresponding to the strong diffraction peak in the XRD test. Furthermore, no second phase is detected besides the wurtzite structure in the samples.

The PL spectrum was investigated to analyze the spectroscopic properties of the ZnO films. A He-Cd laser with a wavelength of 325 nm was chosen as the excitation light source. Figure 2(a) illustrates the PL spectra of the sample films annealed for 1 h at different temperatures in nitrogen.

A typical UV emission around 390 nm was detected; this was attributed to the free exciton transitions. In addition, an obvious emission band covering the visible region was apparent. The blue fluorescence emission around 475 nm was the most remarkable among the bands that appeared in this experiment. Defects are usually thought to be a key factor of DL emissions because they can generate impurity bands into the bandgap[24]. According to Ref. [14], the zinc interstitials in the depletion layer were thought to be the source of blue fluorescence, but there was no blue emission in the thicker films. In this experiment, the blue PL spectrum was found in the thicker films via thermal treatment. In the meantime, multiple visible emission bands were detected. Therefore, it is confirmed that there are abundant defects in the samples. Especially for sputtered metal oxide semiconductor films, oxygen vacancy (V_o) is the most common defect found because oxygen has a larger divergence angle than metal during sputtering, and the formation enthalpy of V_o is fairly low compared with other types of defects, such as interstitial and antisite[13,15].

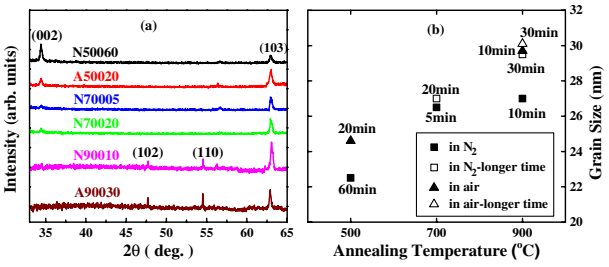

Fig. 1. (a) The XRD patterns of the ZnO films under different annealing conditions. (b) The grain size of films annealed at different temperatures and the time calculated from peak (103).

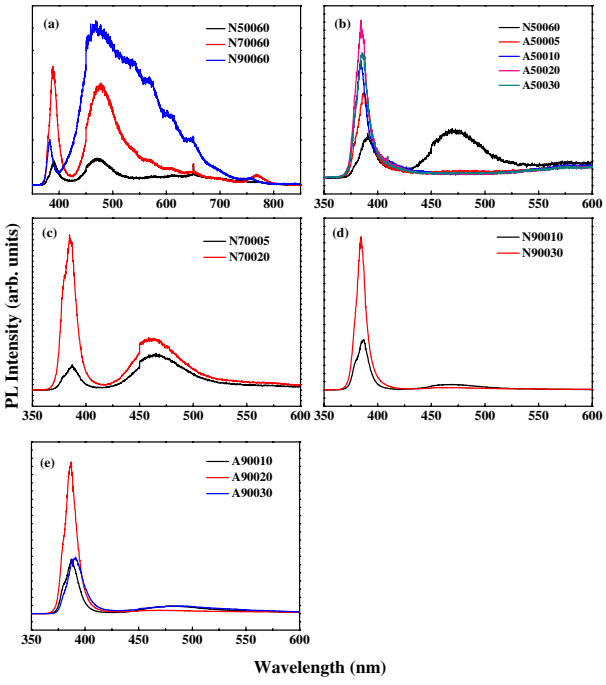

Fig. 2. PL spectra of the films under different annealing conditions: (a) at different temperatures in nitrogen, (b) at 500°C in air, (c) at 700°C in nitrogen, (d) at 900°C in nitrogen, and (e) at 900°C in air.

For as-deposited zinc-rich films, the annealing process primarily influences the concentration of V_o both in nitrogen and in air. Thus, V_o is the major defect in these samples. Although Zn_i should also exist in the films, it should not be significant because its formation enthalpy is higher than that of V_o[6]. With the rising annealing temperature, the peak intensities around 475 nm are enhanced distinctly, as seen in Fig. 2(a). This indicates that more V_o would be generated in this process. When the films are annealed in nitrogen, no external O atoms can be captured for the recombination of V_o. Also, with an increase in the annealing temperature, a fraction of the O atoms could separate out of the films, thus increasing the concentration of V_o. Meanwhile, thermal treatment can make the crystallinity in a sample film increased by the atomic relaxation effect.

Figure 2(b) shows the comparison between the samples annealed at 500°C in air and one in nitrogen. Clearly, after being annealed in air, the fluorescence peak around 475 nm is suppressed sufficiently. If the annealing atmosphere is air, both the supplement of oxygen in air and chemisorption neutralize a part of the V_o and decrease the concentration of V_o. Figures 2(c)–2(e) show the PL spectra of the film samples annealed at 700°C and 900°C. Changes in the intensity of the NBE emission can be observed for the films annealed for different times. This can be explained as follows: those as-deposited films are amorphous. The annealing process leads to their crystallization. Enough annealing time is beneficial for a better crystalline quality, which will generate a stronger NBE emission. At the same time, the annealing process generates and neutralizes defects in the films. Therefore, at a certain annealing temperature, different annealing times influence different concentrations of defects and various qualities of crystalline. Fortunately, it is the stable defect state instead of the complicated crystalline process that influences the PL property of films. X ray photoelectron spectroscopy (XPS) is an effective method for getting defect information from a film sample.

Figures 3(a)–3(j) show the XPS profiles of the oxygen element in the samples. The O 1s peak can be consistently fitted by two Gaussian peaks centered at 529.8 eV (peak 1) and 531.5 eV (peak 2)[25–27]. The component on the lower binding energy of 529.8 eV is attributed to the O^{2-} ions in the hexagonal wurtzite array, which is surrounded by Zn atoms with their full complement of the nearest-neighbor O^{2-} ions. The intensity of this peak is a measure of the oxygen elements in a fully oxidized stoichiometric surrounding. Another peak with a higher binding energy of 531.5 eV is associated with the O^{2-} ion in an oxygen-deficient region within a lattice of ZnO. Therefore, the concentration variation of oxygen defects will cause differences in the peaks at 531.5 eV.

Figure 3(k) shows the profiles of the zinc element in the same two samples. The Zn 2p peak positions of the samples are almost the same. Thus, by inference, the blue fluorescence emission around 475 nm is not due to the zinc-associated defects, such as V_{Zn}, Zn_i, or Zn_o.

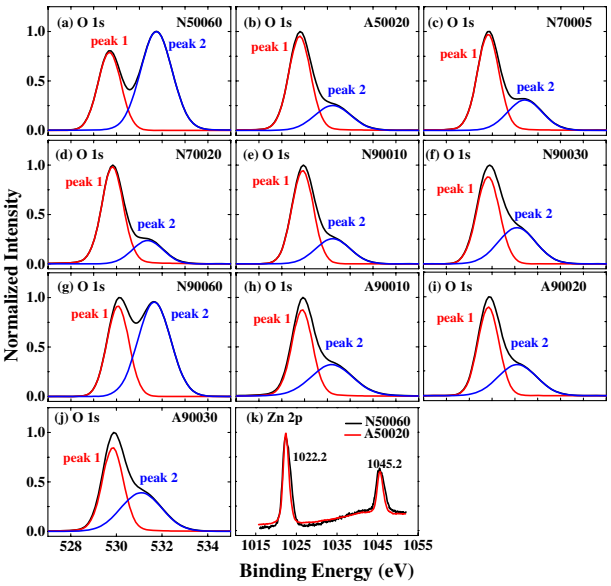

Fig. 3. XPS profiles. (a)–(j) Oxygen and (k) zinc elements in the chosen samples.

To some extent, the ratio of the area under the two O 1s peaks (S_{peak2}/S_{peak1}) indicates the concentration of V_o. The peak intensity ratio of the blue and UV (I_{Blue}/I_{uv}) emissions can easily be calculated, indicating the ratio of the defect region to the area free from defect. The variation trends of the two ratios are similar, as seen in Fig. 4. These results support the hypothesis that the blue fluorescence emission is mainly induced by V_o.

The comparison results of the XPS peak area ratio of S_{peak2}/S_{peak1} (R_{XPS}) and the PL peak intensity ratio of I_{Blue}/I_{uv} (R_{PL}) are illustrated in Fig. 4. It shows a perfect match between the variation trend of R_{XPS} and that of R_{PL}. This is powerful evidence confirming the blue PL, which is strongly associated with V_o. Additionally, the Zn 2p peaks of these samples display little difference, as shown in Fig. 3(k). In this investigation, the Zn 2p peaks are almost the same for all of the samples, while

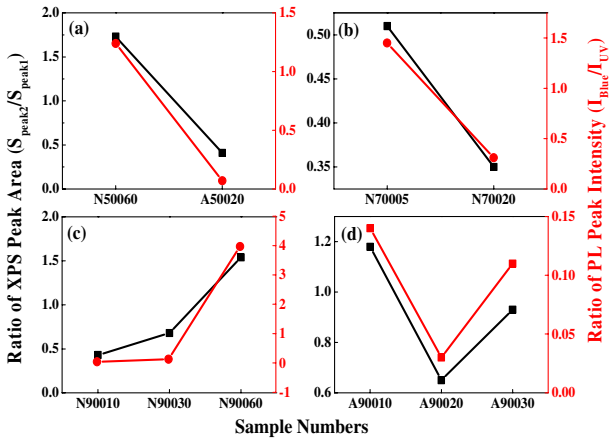

Fig. 4. Comparison of the variation trend of R_{XPS} and that of R_{PL} in the ZnO films.

the O 1s peaks change with the same trend in the blue fluorescence intensity.

In conclusion, a series of ZnO films deposited by magnetron sputtering exhibit hexagonal wurtzite structures and different PL characteristics after undergoing thermal treatment under different conditions. In the experimental investigation, besides the well-known UV emission, a distinct blue fluorescence around 475 nm is found in the films annealed in nitrogen, together with several weak but visible PL emissions. The remarkable UV emission is related to the free exciton effect. The distinct blue PL emission varies under different annealing conditions. Through a detailed analysis of the PL spectrum and the results of the XPS test, we believe that the blue PL emission of the ZnO film is induced by oxygen vacancies.

This work was supported by the Natural Science Foundation of Shanghai (No. 13ZR1402600), the National Natural Science Foundation of China (No. 60578047), the National "973" Program of China (Nos. 2012CB934303 and 2009CB929201), the Shanghai Commission of Science and Technology (No. 06DJ14007), the National "02" Project of China (No. 2011ZX02402), and the Natural Science Foundation of Shandong Province (No. 2011ZRFL019).

References

1. C. G. Van de Walle, Phys. B **308–310**, 899 (2001).
2. A. F. Kohan, G. Ceder, D. Morgan, and C. G. Van de Walle, Phys. Rev. B **61**, 15019 (2000).
3. Z. Wang, D. Wang, F. Huang, and F. Xu, Chin. Opt. Lett. **12**, 093101 (2014).
4. M. H. Huang, S. Mao, H. Feick, H. Yan, Y. Y. Wu, H. Kind, E. Weber, R. Russo, and P.-D. Yang, Science **292**, 1897 (2001).
5. H. Cao, J. Y. Xu, D. Z. Zhang, S. H. Chang, S. T. Ho, E. W. Seelig, X. Liu, and R. P. H. Chang, Phys. Rev. Lett. **84**, 5584 (2000).
6. J. J. Cole, X. Y. Wang, R. J. Knuesel, and H. O. Jacobs, Nano Lett. **8**, 1477 (2008).
7. Z. R. Tian, J. A. Voigt, J. Liu, B. Mckenzie, M. J. McDermott, M. A. Rodriguez, H. Konishi, and H. F. Xu, Nat. Mater. **2**, 821 (2003).
8. A. Thankappan, S. Thomas, and V. P. N. Nampoori, Chin. Opt. Lett. **11**, 101801 (2013).
9. K. Johnston, M. Henry, D. McCabe, E. McGlynn, M. Dietrich, E. Alves, and M. Xia, Phys. Rev. B **73**, 165212 (2006).
10. A. Teke, Ü. Özgür, S. Doğan, X. Gu, H. Morkoç, B. Nemeth, J. Nause, and H. Everitt, Phys. Rev. B **70**, 195207 (2004).
11. S. Cho, J. Ma, Y. Kim, Y. Sun, G. K. L. Wong, and J. B. Ketterson, Appl. Phys. Lett. **75**, 2761 (1999).
12. H. Cao, Y. G. Zhao, S. T. Ho, E. W. Seelig, Q. H. Wang, and R. P. H. Chang, Phys. Rev. Lett. **82**, 2278 (1999).
13. Ü. Özgür, Y. I. Alivov, C. Liu, A. Teke, M. A. Reshchikov, S. Doğan, V. Avrutin, S. J. Cho, and H. Morkoç, J. Appl. Phys. **98**, 041301 (2005).
14. J. C. Moore, L. R. Covington, and R. Stansell, Phys. Status Solidi A **209**, 741 (2012).
15. Y. W. Heo, D. P. Norton, and S. J. Pearton, J. Appl. Phys. **98**, 073502 (2005).
16. X. H. Li, Y. Zhang, and X. J. Ren, Opt. Express **17**, 8735 (2009).
17. S. A. Studenikin and M. Cocivera, J. Appl. Phys. **91**, 5060 (2002).
18. O. F. Schirmer and D. Zwingel, Solid State Commun. **8**, 1559 (1970).
19. B. X. Lin, Z. X. Fu, and Y. B. Jia, Appl. Phys. Lett. **79**, 943 (2001).
20. X. L. Wu, G. G. Siu, C. L. Fu, and H. C. Ong, Appl. Phys. Lett. **78**, 2285 (2001).
21. R. Vidya, P. Ravindran, H. Fjellvåg, B. Svensson, E. Monakhov, M. Ganchenkova, and R. Nieminen, Phys. Rev. B **83**, 045206 (2011).
22. R. Dingle, Phys. Rev. Lett. **23**, 579 (1969).
23. J. M. Li, L. G. Dai, X. P. Wan, and X. L. Zeng, Appl. Phys. Lett. **101**, 173105 (2012).
24. S. Lany and A. Zunger, Phys. Rev. Lett. **98**, 045501 (2007).
25. H. T. Cao, Z. L. Pei, J. Gong, C. Sun, R. F. Huang, and L. S. Wen, J. Solid State Chem. **177**, 1480 (2004).
26. J. C. C. Fan and J. B. Goodenough, J. Appl. Phys. **48**, 3524 (1977).
27. Z. L. Pei, M. Chen, C. Sun, L. S. Wen, and X. Wand, Mater. Lett. **48**, 194 (2001).